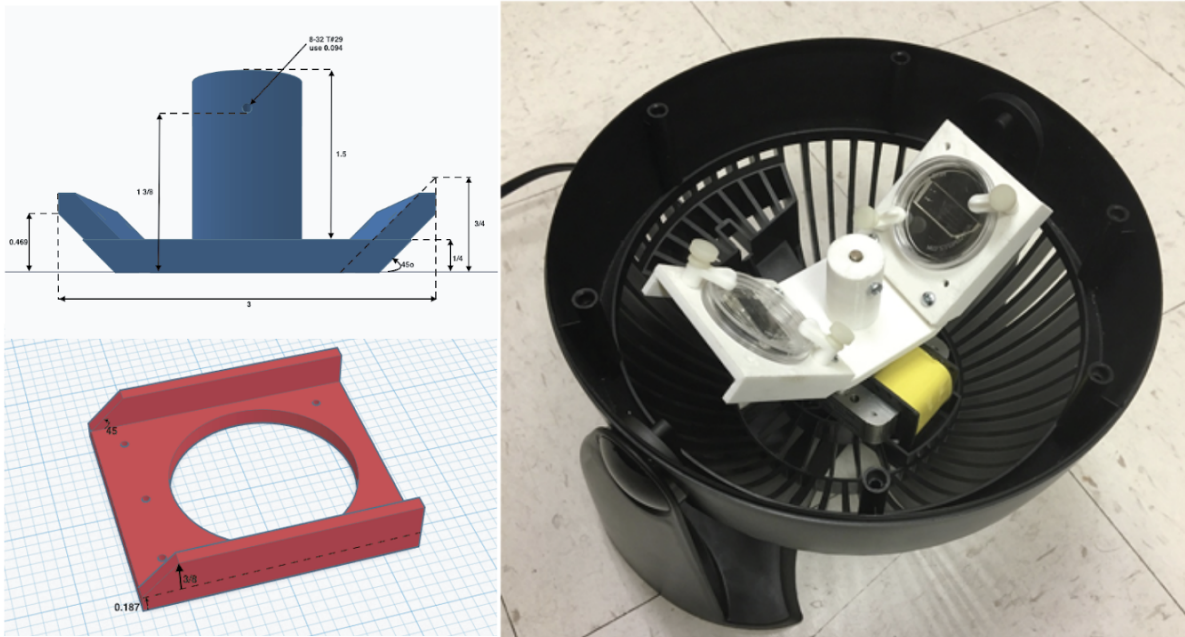


494 Table S1: MM3 parameter values for processed external datasets. Parameters which were changed from the default values are **495** shaded in yellow. Ollion et al., Jug et al. and Sachs et al. datasets were segmented with the non-learning method, while the Lugagne **496** et al. dataset was segmented using the U-Net method.

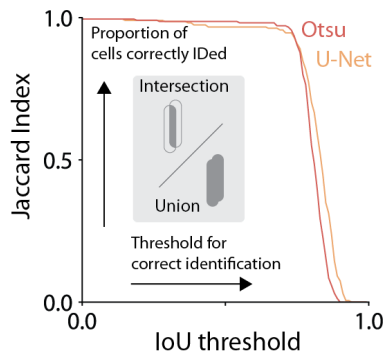
		Default value	Ollion et al.	Lugagne et al.	Jug et al.	Sachs et al.
Compile	Channel width (px)	10	20	10	10	10
	Channel separation (px)	45	90	45	45	45
Subtract	Align pad (px)	10	10	10	10	10
Segment	1st opening (px)	2	3	N/A	3	3
	Distance threshold (px)	2	3	N/A	3	3
	2nd opening (px)	1	2	N/A	1	2
	Otsu threshold scale	1	1.2	N/A	1.0	1.0
	Min object size (px ²)	25	25	25	25	25
Track	Growth length ratio (min, max)	(0.8, 1.3)	(0.9, 1.5)	(0.8, 1.3)	(0.8, 1.3)	(0.8, 1.3)
	Growth area ratio (min, max)	(0.8, 1.3)	(0.9, 1.5)	(0.8, 1.3)	(0.8, 1.3)	(0.8, 1.3)
	Lost cell time (frames)	3	3	3	3	3
	New cell y cutoff (px)	150	300	150	150	150



601

602 Figure S1. Inexpensive fabrication of cell loader with 3D printing.

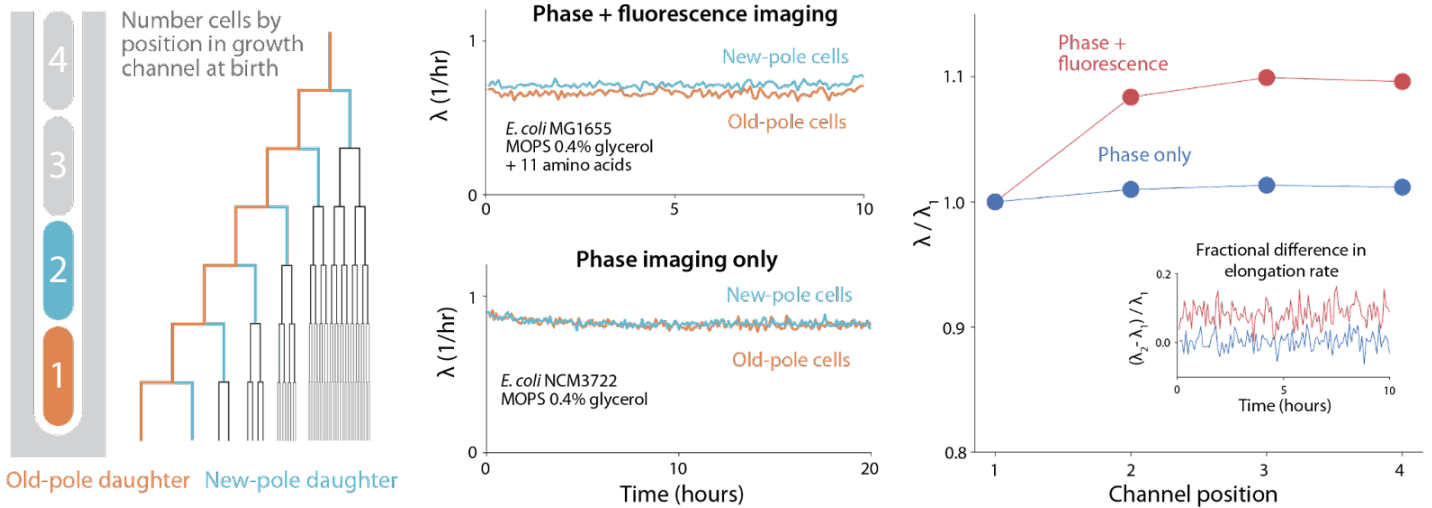
603 An inexpensive device for loading cells into the mother machine. The construction involves 3D printing a custom holder/
604 rotor for a 50mm WillCo dish, on which a mother machine is attached. The holder is printed in three parts (2 blades and a
605 central base) to account for 3D printers with small printing areas. This piece is then assembled and secured to a
606 Honeywell fan from which the original blade has been removed. CAD files and details of the fan centrifuge construction
607 are available at [28].



608

609 **Figure S2: Evaluating segmentation output of napari-MM3 Otsu and U-Net methods**

610 To evaluate the quality of the segmentation masks generated by MM3's Otsu and U-Net segmentation methods, we
611 computed the Jaccard index [42,51] as a function of the intersection-over-union (IoU) threshold.



612

613 Figure S3: Old-pole aging phenotype is strain specific. Cells imaged with fluorescence often show signs of aging in the
 614 old-pole “mother” cell. For instance, in the dataset analyzed in Figure 4 (*E. coli* MG1655 with the fluorescent protein YPet fused
 615 to DnaN), we observed systematic differences in cell elongation rate and size between the old-pole cell at the end of the growth
 616 channel and its sisters, which inherit the new pole (top center). However, this asymmetry is not universal. Using napari-MM3’s
 617 Otsu segmentation method, we re-analyzed previously published data obtained without fluorescence illumination [32], and found
 618 that the old-pole and new-pole cell elongation rates varied only on the order of 1% (lower center), while in the dataset obtained
 619 under fluorescence imaging, the old-pole mother cells grow 7-10% slower than the new pole cells. Cells born third or fourth from
 620 the closed end of the channel also grow slower than the old-pole mother (right). The asymmetry in growth rate between old-pole
 621 and new pole cells persists across time (right, inset). These results are consistent with a previous survey [63], which found that
 622 most evidence for aging in *E. coli* comes from studies utilizing fluorescent proteins for visualization.

623